THE STRUCTURES OF TWO NOVEL Sn^{2+} OXYSALTS FOUND
WITH ROMARCHITE AND HYDROROMARCHITE AS CORROSION PRODUCTS
OF PEWTER ARTIFACTS

Andrew J. LOCOCK[§], Robert A. RAMIK and Malcolm E. BACK

Mineralogy, Department of Natural History, Royal Ontario Museum,
100 Queen's Park, Toronto, Ontario, Canada M5S 2C6

Abstract

The crystal structures of an anthropogenic Sn^{2+} silicate, Sn$_6$O$_4$(SiO$_4$), hexagonal, space group $P6_3mc$, a 7.3742(4), c 11.9598(10) Å, V 563.23(6) Å^3, $Z = 2$, D_{calc} 5.12 g/cm^3, and an anthropogenic Sn^{2+} sulfate, Sn$_6$O$_4$(SO$_4$)(OH)$_2$, orthorhombic, space group $Pbca$, a 14.0071(8), b 12.5016(7), c 14.5030(9) Å, V 2539.6(3) Å^3, $Z = 8$, D_{calc} 4.74 g/cm^3, were refined by full-matrix least-squares techniques on the basis of F^2 to agreement indices $R1$ (Sn^{2+} silicate and Sn^{2+} sulfate) of 3.0 and 4.2%, calculated for 704 and 3281 unique observed reflections ($|F_o| \geq 4\sigma_F$), and wR_2 of 5.5 and 11.0% for all data, respectively. Intensity data were collected at room temperature using Mo$K\alpha$ radiation and a CCD-based area detector. Both structures contain the [Sn$_6\phi_8$] cluster [ϕ: O^{2-} or (OH)$^-$], which has been found in several stannous compounds, and which can be derived from the structure of fluorite. These two compounds occur with romarchite, SnO, and hydroromarchite, Sn$_3$O$_2$(OH)$_2$, on pewter bowls that had become corroded in cold freshwater for approximately 160 years.

Keywords: romarchite, hydroromarchite, stannous compounds, tin compounds, corrosion, pewter, non-merohedral twin, silicate, sulfate, fluorite derivative, crystal structure.

Sommaire

Nous avons affiné la structure cristalline d'un silicate de Sn^{2+} anthropogénique, Sn$_6$O$_4$(SiO$_4$), hexagonal, groupe d'espace $P6_3mc$, a 7.3742(4), c 11.9598(10) Å, V 563.23(6) Å^3, $Z = 2$, D_{calc} 5.12 g/cm^3, et un sulfate de Sn^{2+} anthropogénique, Sn$_6$O$_4$(SO$_4$)(OH)$_2$, orthorhombique, groupe d'espace $Pbca$, a 14.0071(8), b 12.5016(7), c 14.5030(9) Å, V 2539.6(3) Å^3, $Z = 8$, D_{calc} 4.74 g/cm^3, par techniques de moindres carrés sur matrice entière en utilisant les facteurs F^2, jusqu'à un résidu $R1$ (silicate et sulfate) de 3.0 et 4.2% calculé pour 704 et 3281 réflexions uniques observées ($|F_o| \geq 4\sigma_F$), et une valeur de wR_2 égale à 5.5 et 11.0% pour toutes les données, respectivement. Les données d'intensité ont été prélevées à température ambiante avec rayonnement Mo$K\alpha$ et un détecteur à aire de type CCD. Les deux structures contiennent des groupes [Sn$_6\phi_8$], ϕ correspondant à O^{2-} ou (OH)$^-$, dérivés de la structure de la fluorite, tout comme dans plusieurs composés d'étain bivalent. On trouve ces deux composés associés à la romarchite, SnO, et la hydroromarchite, Sn$_3$O$_2$(OH)$_2$, sur des bols en alliage d'étain devenus corrodés suite à leur submersion dans l'eau fraîche froide pour environ 160 ans.

(Traduit par la Rédaction)

Mots-clés: romarchite, hydroromarchite, composés stanneux, composés d'étain, corrosion, alliage d'étain, macle non méro-édrique, silicate, sulfate, dérivé de fluorite, structure cristalline.

[§] *Current address*: Department of Earth and Atmospheric Sciences, University of Alberta, 1-26 Earth Sciences Building, Edmonton, Alberta, Canada T6G 2E3. *E-mail address*: alocock@ualberta.ca

INTRODUCTION

The occurrence of compounds of divalent tin and oxygen in natural settings is quite uncommon. Tin itself is not a particularly abundant element in the continental crust, with an abundance estimated to be similar to that of Be or Pt at ~1.7 ppm (Rudnick & Gao 2003). The mineralogy of tin is dominated by intermetallic compounds, sulfides, oxysalts and oxides (Mandarino & Back 2004), of which cassiterite, SnO_2, is by far the most common species. Of the 77 minerals that are known to contain essential tin, only 31 also require essential oxygen, the majority of which contain tin in the tetravalent state. Only six minerals require both oxygen and divalent tin: abhurite [$Sn_{21}O_6(OH)_{14}Cl_{16}$], foordite [$SnNb_2O_6$], hydroromarchite [$Sn_3O_2(OH)_2$], romarchite [SnO], stannomicrolite [$Sn_2Ta_2O_7$], and thoreaulite [$SnTa_2O_6$] (Mandarino & Back 2004, von Schnering *et al.* 1981).

In general terms, these six minerals form in one of two distinct environments: granitic pegmatites (foordite, stannomicrolite and thoreaulite), and low-temperature corrosion (abhurite, hydroromarchite and romarchite). Černý *et al.* (1988) reviewed the occurrence of divalent-tin minerals in granitic pegmatites, and concluded that conditions of exceptionally low oxygen fugacity are required for their formation. Abhurite, hydroromarchite and romarchite generally have an anthropogenic origin, being derived from the corrosion of tin, bronze, or pewter artifacts (Ramik *et al.* 2003), commonly in a marine environment, *e.g.*, relics on sunken ships (Dunkle *et al.* 2003, 2004). Rarely, romarchite occurs as a natural (non-anthropogenic) product from the alteration of native tin, or as a replacement of the tin sulfide herzenbergite (*cf.* Ramik *et al.* 2003). In the type material, romarchite occurs as a fine-grained black pseudomorph after a lower-symmetry species (Ramik *et al.* 2003); the precursor is likely to have been the metastable orthorhombic polymorph of romarchite, red stannous oxide (*cf.* Donaldson *et al.* 1961, 1963, Donaldson 1964). Natural hydroromarchite has been reported to occur in massive sphalerite–pyrite ore at the Corchia mine, western Emilia Romagna, Italy (Garuti & Zaccarini 2005).

Ramik *et al.* (2003) described two unknown tin-bearing phases (UTP–1 and UTP–2) that occur with type material of romarchite and hydroromarchite; for the two unknowns, they listed the strongest reflections of their powder X-ray-diffraction patterns and presented SEM images. We have determined the structures of these phases: UTP–1 is a novel Sn^{2+} sulfate, $Sn_6O_4(SO_4)(OH)_2$, which occurs as thin white plates, and UTP–2 is a novel Sn^{2+} silicate, $Sn_6O_4(SiO_4)$, which occurs as stubby yellow hexagonal prisms. Along with romarchite and hydroromarchite, these stannous compounds resulted from the corrosion of pewter bowls in five meters of cold freshwater. The bowls had been lost for approximately 160 years below the rapids at Boundary Falls, on the Winnipeg River, Kenora District, Ontario, at latitude 50°13'15"N, longitude 95°06'12"W (Ramik *et al.* 2003). The Commission on New Minerals and Mineral Names (CNMMN) of the International Mineralogical Association approved two of the corrosion products as the new mineral species romarchite and hydroromarchite in 1969 despite their anthropogenic origin (Organ & Mandarino 1971, Ramik *et al.* 2003). However, since that time, the CNMMN has modified its procedures such that compounds formed by the action of water on anthropogenic substances are no longer accepted as minerals (Nickel 1995, Nickel & Grice 1998); the status of such compounds that were accepted in the past as minerals remains unchanged. As a result, the Sn^{2+} silicate and Sn^{2+} sulfate are described here as artificial substances, not as mineral species, in contrast to romarchite and hydroromarchite. Incrustations of the Sn^{2+} silicate and Sn^{2+} sulfate occur in relative abundance on the pewter bowl registered under catalogue number M49593 in the mineral collections of the Royal Ontario Museum. The Sn^{2+} sulfate, $Sn_6O_4(SO_4)(OH)_2$, differs in stoichiometry and structure from the stannous oxide sulfate hydroxide, $Sn_3O(SO_4)(OH)_2$, previously reported (Davies & Donaldson 1967, Grimvall 1975, Edwards *et al.* 1996).

ORIGIN OF THE Sn^{2+} COMPOUNDS

The Eh–pH conditions of freshwater streams are relatively oxidizing (Garrels & Christ 1965), and are consistent with the formation of stannic compounds such as cassiterite, rather than stannous compounds, which require a much more reducing environment (Sèby *et al.* 2001). Indeed, the outermost surfaces of some of the pewter bowls lost at Boundary Falls are coated mainly with cassiterite (Ramik 2004). The occurrence of stannous compounds at this locale is sharply defined, and limited to the small volume enclosed by the nesting bowls. This restricted volume was apparently buffered to reducing conditions by the abundant metallic tin of the pewter. Over the course of time, the formation of corrosion phases of tin cemented some of the nested bowls together, sealing the enclosed spaces (Ramik 2004).

The source(s) of the Si and S necessary to form the Sn^{2+} silicate and Sn^{2+} sulfate are not known with certainty. Worldwide, river water averages only 13.1 ppm Si and 11.2 ppm SO_4^{2-} (Livingstone 1963). It is possible that glass beads found in intimate association with the pewter artifacts at Boundary Falls acted as the source; qualitative SEM–EDS and XRF examination of a bead showed that it contains major amounts of Si, Ca, and K, with lesser Cl, S, Al, Mg, Na and possibly P. Tin-bearing alteration-induced phases immediately beside the beads contain significant levels of Si and S; their proximity is consistent with the beads being the likely source of these elements.

Experimental

Composition

The qualitative chemical compositions of the Sn^{2+} silicate and the Sn^{2+} sulfate were examined with a NanoLab 7 scanning electron microscope (SEM) equipped with an Si(Li) energy-dispersive spectrometer (EDS). Quantitative analyses were not obtained. The presence of Sn and of Si (and of minor S) in the Sn^{2+} silicate, and Sn and S in the Sn^{2+} sulfate, was confirmed. No other elements with Z > 11 were detected.

Single-crystal X-ray diffraction

For each stannous compound, an apparently optically homogeneous crystal was mounted on a Bruker PLAT-FORM three-circle X-ray diffractometer operated at 50 keV and 40 mA and equipped with a 4K APEX CCD detector with a crystal-to-detector distance of 4.7 cm. Data were collected at room temperature using graphite-monochromatized MoKα X-radiation and frame widths of 0.3° in ω. Details of the data acquisition and refine-

ment parameters are provided in Table 1; the formulas of these compounds are expressed as [Sn$_6$O$_6$(OH)$_2$]SO$_2$ and [Sn$_6$O$_8$]Si in Table 1 in order to emphasize the presence of the [Sn$_6\phi_8$] cluster in the structure, in which φ represents O^{2-} or (OH)$^-$. The intensity data were reduced and corrected for Lorentz, polarization, and background effects using the program SAINT (Bruker 1998a), and the unit-cell dimensions were refined using least-squares techniques. Comparison of the intensities of equivalent reflections measured at different times during data acquisition showed no significant decay for any of the compounds.

Systematic absences of reflections for the Sn^{2+} sulfate are consistent solely with space group *Pbca*. Systematic absences of reflections for the Sn^{2+} silicate are consistent with space groups *P6$_3$/mmc*, *P6$_3$mc*, *P$\bar{6}$2c*, *P$\bar{3}$1c*, or *P31c*. Assigning phases to a set of normalized structure-factors with the E-stats routine in the WINGX software package (Farrugia 1999) gave a mean value of |E^2 − 1| of 0.708, indicative of a non-centrosymmetric space-group. Interestingly, Ramik *et al*. (2003) noted that the Sn^{2+} silicate has a powder X-ray-diffraction pattern that is "remarkably similar to that of the sulfosalt pearceite", whose structure has recently been reported in space group *P$\bar{3}$m1*, *a* 7.3876(4), *c* 11.8882(7) Å (Bindi *et al*. 2006). In addition, the stoichiometric ratios of the analyzed pearceite, (Ag$_{13.03}$Cu$_{2.97}$)$_{\Sigma 16}$(As$_{1.18}$Sb$_{0.82}$)$_{\Sigma 2}$S$_{11}$, are comparable to those of the Sn^{2+} silicate (expressed as O$_{16}$Si$_2$Sn$_{12}$), although their structures differ considerably in detail.

Scattering curves for neutral atoms, together with anomalous dispersion corrections, were taken from *International Tables for X-ray Crystallography, Vol. C* (Wilson 1992). The SHELXTL Version 5 series of programs was used for the solution and refinement of the crystal structures (Sheldrick 1998).

Structure refinement

Both structures were refined on the basis of *F*^{2} for all unique data. As is common in heavy-atom structures, the location of each H atom in the unit cell of the Sn^{2+} sulfate was not determined because of the minimal contribution of H atoms to the diffracted intensities.

To avoid refinement of a model of the Sn^{2+} silicate structure in an incorrect hexagonal or trigonal space-group, the unit cell of the Sn^{2+} silicate was transformed to a monoclinic *C*-centered setting, solved in space group *Cm* by direct methods (Schenk 1984), and refined to an agreement index (*R*1) of 3.7%. This solution was transformed to space group *P6$_3$mc* by use of the ADDSYM algorithm in the program PLATON (Le Page 1987, Spek 2003). A structure model including anisotropic displacement parameters for all atoms converged, and gave an agreement index (*R*1) of 3.0%, calculated for the 704 observed unique reflections (|F$_o$| ≥ 4σ$_F$). The final value of *wR*$_2$ was 5.5% for all data using the structure-factor

TABLE 1. CRYSTALLOGRAPHIC DATA AND REFINEMENT PARAMETERS

Compound	Sn^{2+} silicate	Sn^{2+} sulfate	
a (Å)	7.3742(4)	14.0071(8)	
b (Å)		12.5016(7)	
c (Å)	11.9598(10)	14.5030(9)	
V (Å^3)	563.23(6)	2539.6(3)	
Space group	*P6$_3$mc*	*Pbca*	
Z	2	8	
Formula	[Sn$_6$O$_8$]Si	{Sn$_6$O$_6$(OH)$_2$}SO$_2$	
Formula weight	868.34(2)	906.34(2)	
F(000)	756.0	3184.0	
μ (mm^{-1})	13.22	11.82	
D$_{calc}$ (g/cm^3)	5.12	4.74	
Crystal size (mm)	0.04 × 0.04 × 0.04	0.16 × 0.10 × 0.02	
Color and habit	pale yellow hexagonal prism	white plate	
Temperature (K)	293(2)	293(2)	
Frame width (°), time (s)	0.3, 60	0.3, 100	
Collection, hours	hemisphere, 24	sphere, 72	
θ range	3.19 – 34.57	2.60 – 34.53	
Data collected	-7 ≤ h ≤ 11, k ±11, -18 ≤ l ≤ 17	-22 ≤ h ≤ 21, k ± 19, l ± 23	
Absorption*	ellipsoid	plate (100), 3°	
Total reflections	5876	43473	
Unique refl., *R*$_{int}$	917, 4.4%	5329, 6.3%	
Unique |F$_o$| ≥ 4σ$_F$	704	3281	
Parameters	35	209	{124}
*R*1† for |F$_o$| ≥ 4σ$_F$	3.0%	4.2%	{9.1%}
*R*1‡ all data, *wR*$_2$‡	4.4, 5.5%	7.8, 11.0%	{12.3, 23.4%}
Weighting *a*	0.0220	0.054	{0.154}
Goodness of fit	0.862	0.929	{0.969}
Mean shift/esd	0.000	0.000	
Peaks (*e*/Å^3)	2.4, -0.9	5.9, -3.2	{17.3, -2.6}

* Correction for absorption is semi-empirical (crystal modeled either as an ellipsoid, or as a plate with rejection of data within 3° of the primary X-ray beam).
† *R*1 = [Σ||F$_o$| − |F$_c$||] / Σ|F$_o$| × 100.
‡ *wR*$_2$ = {Σ[*w*(F$_o^2$ − F$_c^2$)^2] / Σ[*w*(F$_o^2$)^2]}$^{0.5}$ × 100, *w* = 1/(σ^2(F$_o^2$) + (*a•P*)^2, and *P* = ⅓ max(0, F$_o^2$) + ⅔ F$_c^2$.
Parameters enclosed in {} refer to the preliminary model that does not account for the presence of non-merohedral twinning; see text.

weights assigned during least-squares refinement. The positional parameters are given in Table 2.

The structure of the Sn^{2+} sulfate was solved in space group *Pbca* by direct methods (Schenk 1984), and a preliminary model of the structure including anisotropic displacement parameters for Sn, S, and the four O positions that directly coordinate S converged, yielding an agreement index ($R1$) of 9.1%, calculated for the 3281 observed unique reflections ($|F_o| \geq 4\sigma_F$). The final value of wR_2 for this model was 23.4% for all data using the structure-factor weights assigned during least-squares refinement. Six large peaks were present in the difference-Fourier map, at positions inconsistent with additional sites. As detailed below in the Description of the Structures, the crystal investigated

is interpreted to be a non-merohedral twin, twinned by 180° rotation about the [$\bar{1}$20] direction, and having a highly asymmetrical distribution of the twin domains. The six large difference-Fourier peaks are interpreted to result from the unmodeled influence (in the preliminary structure-model) of the array of six Sn positions that belong to the smaller twin-domain. We were unable to resolve the orientation of each twin-domain with the powerful indexing program GEMINI (Bruker 1998b). Rather, the six positions were included in the structure model as additional Sn atoms, sites $A(1) - A(6)$ in Table 3, attributed to a separate twin-domain, and their site occupancy refined by a single scale-factor. In this fashion, the geometrical relationship between the twin components, as well as their relative proportion, have been estimated. The final structure-model, including anisotropic displacement parameters for all atoms, converged and gave an agreement index ($R1$) of 4.2%, calculated for the 3281 observed unique reflections ($|F_o| \geq 4\sigma_F$). The final value of wR_2 was 11.0% for all data using the structure-factor weights assigned during least-squares refinement.

The positional parameters of atoms in the Sn^{2+} silicate and the Sn^{2+} sulfate are given in Tables 2 and 3, and selected interatomic distances are in Tables 4 and 5, respectively. Observed and calculated structure-factors, and anisotropic displacement parameters, are available from the Depository of Unpublished Data, CISTI, National Research Council, Ottawa, Ontario K1A 0S2, Canada.

Bond-valence sums at the non-H cation sites for each compound are listed in Tables 6 and 7, respectively, and were calculated using the parameters of Brese & O'Keeffe (1991) for Sn^{2+}, Si^{4+} and S^{6+}. The bond-valence sums for the cations are in good agreement with expected formal oxidation-states.

DESCRIPTION OF THE STRUCTURES

The Sn^{2+} silicate

In the Sn^{2+} silicate, each of the divalent tin atoms is coordinated to four oxygen atoms (Table 4). The coordination environment of the tin atoms is not that of tetrahedra, but rather of a highly distorted pyramid, or a bent "see-saw" with the tin atom as the hinge

TABLE 2. ATOM POSITIONS FOR Sn^{2+} SILICATE

	x	y	z	U_{eq}	Wyckoff position
Sn(1)	0.82637(4)	0.17363(4)	0.59214(6)	0.03065(15)	6c
Sn(2)	0.49272(5)	0.50728(5)	0.85203(4)	0.02947(15)	6c
Si(1)	1/3	2/3	0.5963(4)	0.0146(6)	2b
O(1)	0.4547(4)	0.9094(8)	0.5477(4)	0.0275(13)	6c
O(2)	1/3	2/3	0.7307(8)	0.024(2)	2b
O(3)	2/3	1/3	0.6177(7)	0.0118(17)	2b
O(4)	0.1946(4)	0.3891(7)	0.9208(4)	0.0167(10)	6c

U_{eq} is defined as one third of the trace of the orthogonalized U_{ij} tensor.

TABLE 3. ATOM POSITIONS FOR Sn^{2+} SULFATE

	x	y	z	U_{eq}	Wyckoff position
Sn(1)	0.01749(3)	0.82313(4)	0.33891(3)	0.02042(11)	8c
Sn(2)	0.01109(3)	0.67521(4)	0.54400(3)	0.02078(11)	8c
Sn(3)	0.26344(3)	0.83072(4)	0.45157(3)	0.02085(11)	8c
Sn(4)	0.25365(3)	0.82371(4)	0.16166(3)	0.01995(11)	8c
Sn(5)	0.38223(3)	0.59124(4)	0.45298(3)	0.02045(11)	8c
Sn(6)	0.39966(4)	0.58021(4)	0.15603(3)	0.02378(12)	8c
S(1)	0.14065(12)	0.57227(14)	0.18255(11)	0.0194(3)	8c
O(1)	0.1286(4)	0.4669(4)	0.1349(4)	0.0271(11)	8c
O(2)	0.2167(4)	0.6332(4)	0.1284(4)	0.0282(11)	8c
O(3)	0.0520(4)	0.6293(5)	0.1814(4)	0.0354(13)	8c
O(4)	0.1773(4)	0.5560(5)	0.2772(4)	0.0395(15)	8c
O(5)	0.3845(3)	0.7443(4)	0.1898(3)	0.0147(8)	8c
O(6)H	0.0451(3)	0.6519(4)	0.3851(3)	0.0204(10)	8c
O(7)H	0.3796(3)	0.7455(4)	0.3750(3)	0.0170(9)	8c
O(8)	-0.0107(7)	0.8227(9)	0.4791(5)	0.0173(16)	8c
O(9)	0.3855(4)	0.6096(4)	0.0145(4)	0.0178(10)	8c
O(10)	0.2753(4)	0.8156(4)	0.0202(3)	0.0174(9)	8c
A(1)	-0.0160(4)	0.6752(5)	0.6624(4)	0.0249(14)	8c
A(2)	0.2188(4)	0.8243(5)	0.3384(4)	0.0318(16)	8c
A(3)	0.3337(4)	0.5807(5)	0.3428(4)	0.0258(14)	8c
A(4)	0.2262(5)	0.8250(5)	0.0423(4)	0.0280(14)	8c
A(5)	0.3575(5)	0.5908(5)	0.0471(5)	0.0264(15)	8c
A(6)	-0.0263(9)	0.8322(13)	0.4521(8)	0.028(2)	8c

U_{eq} is defined as one third of the trace of the orthogonalized U_{ij} tensor. Positions $A(1)$ to $A(6)$ result from the presence of non-merohedral twinning. The occupancy of each A position is 9.0(1)% of a tin atom, 4.50(5) *epfu*.

TABLE 4. SELECTED INTERATOMIC DISTANCES (Å) AND ANGLES (°) FOR Sn^{2+} SILICATE

Sn(1)-O(3)	2.0626(14)	Sn(2)-O(4)	2.087(3) ×2
Sn(1)-O(4)	2.067(5)	Sn(2)-O(1)	2.435(5)
Sn(1)-O(1)	2.500(4) ×2	Sn(2)-O(2)	2.500(5)
<Sn(1)-O>	2.28	<Sn(2)-O>	2.28
Si(1)-O(2)	1.607(11)	O(1)-Si(1)-O(1)	108.4(3) ×3
Si(1)-O(1)	1.656(6) ×3	O(2)-Si(1)-O(1)	110.6(2) ×3
<Si(1)-O>	1.64	<O-Si(1)-O>	109.5

FIG. 1. a) Projection of the structure of Sn^{2+} silicate, [Sn$_6$O$_8$]Si along [001]. b) Projection along [010]. The structure may be considered to consist of [Sn$_6$O$_8$] clusters polymerized into a framework by vertex-sharing with silicate tetrahedra. Oxygen positions are shown as red spheres, tin atoms as gray spheres, silicon atoms as blues spheres, and silicate tetrahedra are translucent blue-green. Bonds within the tetrahedra are blue, and bonds outside of tetrahedra are gray.

a)

b)
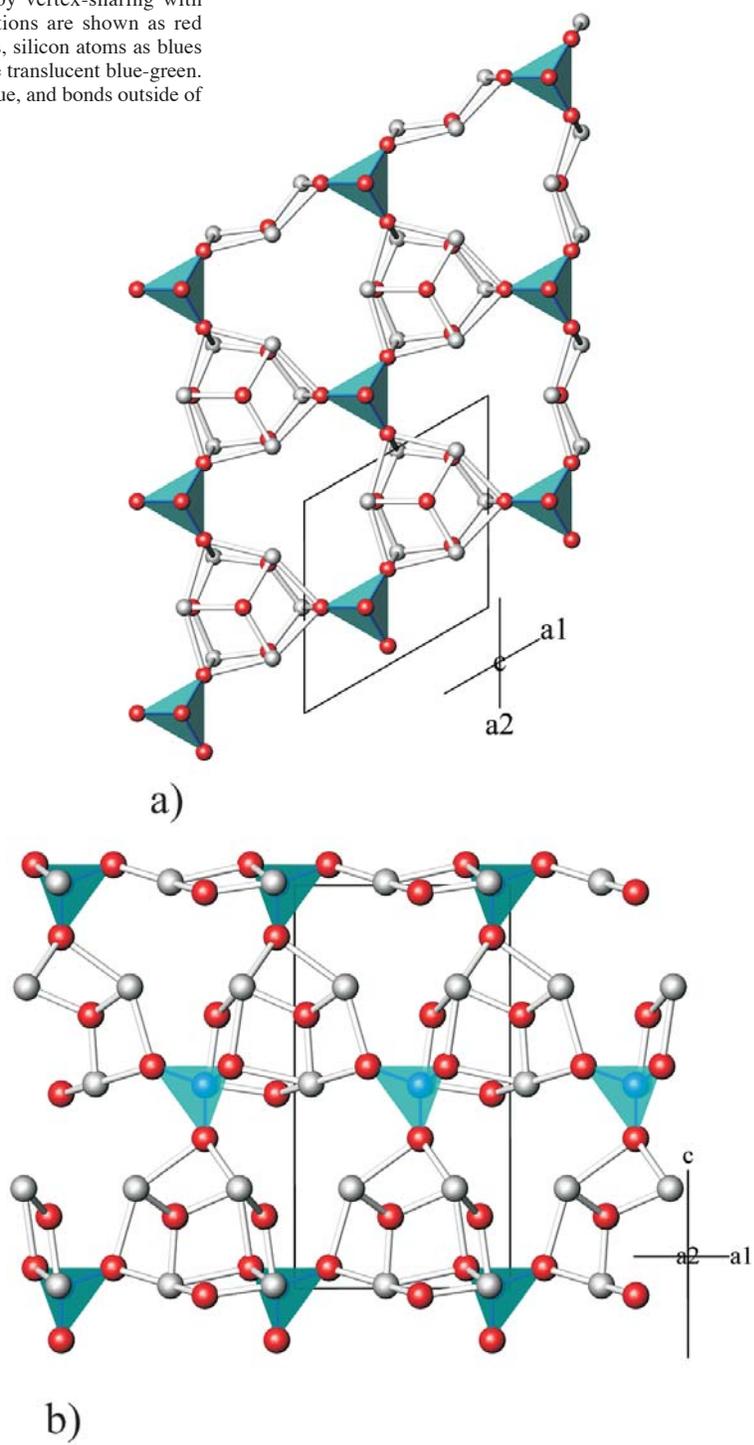
point. This coordination is also referred to as distorted pseudo-trigonal bipyramidal (Harrison 1998). The tin and oxygen atoms form clusters with stoichiometry $[Sn_6O_8]^{4-}$, whose geometry approximates that of a deltoid dodecahedron, $\{hll\}$ in point group $3m$ (Fig. 1). The clusters are connected into a framework structure by sharing vertices with silicate tetrahedra, resulting in open channels along [100] and [001] (Fig. 1). Formally, divalent tin has a $5s^2$ lone pair of electrons in its valence shell, and it is likely that the lone pairs from the tin atoms project into the open channels of the framework.

In order to compare the Sn^{2+} silicate to other structures, it is convenient to adopt an anion-centered representation of tetrahedra, as outlined by Krivovichev & Filatov (1999a, b). Such a representation is particularly useful for comparing metal-rich compounds. In the Sn^{2+} silicate, an OSn_3Si tetrahedron can be defined; four such anion-centered tetrahedra share vertices (tin positions) to form what O'Keeffe & Hyde (1996) referred to as a "supertetrahedron" (Fig. 2a). The supertetrahedron is a common cluster in crystal structures; for example, the unit cell of sphalerite contains a supertetrahedron of four complete SZn_4 tetrahedra. The supertetrahedron can be derived from the anion-centered representation of fluorite (the n module of Krivovichev 1999a). In the case of the supertetrahedron found in the Sn^{2+} silicate, in addition to the four OSn_3Si tetrahedra, four of the faces of the central octahedral cavity are decorated by oxygen in threefold coordination by tin atoms (Fig. 2a). The individual OSn_3Si tetrahedra are quite distorted because of the differences between the O–Si and O–Sn interatomic distances (Table 4). In agreement with the geometrical characteristics for linkage of anion-centered

tetrahedra outlined by Krivovichev & Filatov (1999b), the three short edges of the OSn_3Si tetrahedron (Sn–Sn distance ~3.5 Å, O–Sn distance ~2.5 Å) are shared with OSn_3 triangles (O–Sn distance ~2.1 Å), whereas the Si atom (Si–Sn distance ~3.7 Å, O–Si distance 1.64 Å) is shared as a vertex between four supertetrahedra (*i.e.*, only corner-shared, Fig. 2b). The polymerization of the supertetrahedra through the Si position gives rise to a three-dimensional framework; in this representation of the structure, the open channels are still present along [100] and [001], and can thus accommodate the lone-electron pairs of the tin atoms (Fig. 2b).

The structure of the Sn^{2+} silicate is presented in the non-centrosymmetric space-group $P6_3mc$; the lack of a center of symmetry is most easily demonstrated by the observation that all of the tetrahedra point in the same direction (Fig. 2b). During least-squares refinement, the structure was tested for the presence of twinning by inversion, twin operator [$\bar{1}00/0\bar{1}0/00\bar{1}$]. However, because of the small degree of anomalous scattering by Sn for Mo$K\alpha$ radiation (f' –0.626, f' 1.429; values from the FPRIME routine in the WINGX software package, Farrugia 1999), the inversion twin scale-factor refined to 9(8)%, indicating that the absolute structure cannot be determined reliably with the measured intensity-data.

The Sn^{2+} sulfate

The six Sn positions in the Sn^{2+} sulfate have the same "see-saw"-type coordination as in the Sn^{2+} silicate (Table 5), and together form a similar deltoid dodecahedron of composition $[Sn_6O_6(OH)_2]^{2-}$, two vertices of which are shared with sulfate tetrahedra (Fig. 3a). Analysis of the bond-valence sums of the oxygen atoms of the Sn^{2+} sulfate (Table 7) shows that two positions in the tin–oxygen cluster correspond to hydroxyl groups: O(6)H and O(7)H. Although the hydrogen atoms were not located during structure refinement, the acceptor atoms for the hydrogen bonds can be identified by a combination of distance and bond-valence criteria. Of the non-hydroxyl oxygen atoms, O(3) and O(4) have the lowest bond-valence sums (Table 7), and are within 3.0 Å of the hydroxyl positions (Table 5). Thus, the donor–acceptor pairs involved in hydrogen bonding

TABLE 5. SELECTED INTERATOMIC DISTANCES (Å) AND ANGLES (°) FOR Sn²⁺ SULFATE

Sn(1)-O(8)	2.071(9)	Sn(4)-O(10)	2.076(5)
Sn(1)-O(5)	2.148(4)	Sn(4)-O(5)	2.124(4)
Sn(1)-O(6)H	2.277(5)	Sn(4)-O(1)	2.465(5)
Sn(1)-O(1)	2.751(5)	Sn(4)-O(2)	2.484(5)
<Sn(1)-O>	2.31	<Sn(4)-O>	2.29
Sn(2)-O(8)	2.092(10)	Sn(5)-O(8)	2.092(12)
Sn(2)-O(9)	2.118(5)	Sn(5)-O(10)	2.133(5)
Sn(2)-O(6)H	2.371(5)	Sn(5)-O(7)H	2.236(5)
Sn(2)-O(7)H	2.399(4)	Sn(5)-O(1)	2.740(5)
<Sn(2)-O>	2.25	<Sn(5)-O>	2.30
Sn(3)-O(9)	2.076(5)	Sn(6)-O(9)	2.095(5)
Sn(3)-O(10)	2.089(5)	Sn(6)-O(5)	2.120(4)
Sn(3)-O(7)H	2.240(4)	Sn(6)-O(6)H	2.304(5)
Sn(3)-O(2)	2.685(5)	Sn(6)-O(2)	2.677(5)
<Sn(3)-O>	2.27	<Sn(6)-O>	2.30
S(1)-O(3)	1.432(6)	O(1)-S(1)-O(2)	106.2(3)
S(1)-O(4)	1.479(6)	O(3)-S(1)-O(1)	109.6(3)
S(1)-O(1)	1.497(5)	O(3)-S(1)-O(2)	110.5(3)
S(1)-O(2)	1.527(5)	O(3)-S(1)-O(4)	112.4(3)
<S(1)-O>	1.48	O(4)-S(1)-O(1)	110.3(3)
		O(4)-S(1)-O(2)	107.7(3)
O(6)H...O(4)	2.704(7)	<O-S(1)-O>	109.5
O(7)H...O(3)	2.934(7)		

TABLE 6. BOND-VALENCE ANALYSIS FOR Sn²⁺ SILICATE (*vu*)

	Si(1)	Sn(1)	Sn(2)	Total
O(1)	0.92 ×3↓	0.25 ×2↓→	0.26	1.72
O(2)	1.05		0.25 ×3→	1.80
O(3)		0.81 ×3 →		2.43
O(4)		0.80	0.76 ×2↓→	2.32
Total	3.81	2.11	2.07	

The symbols ↓ and → indicate that summation is carried out multiple times in the direction(s) indicated, and once in the other direction.

are expected to be O(6)H...O(4) and O(7)H...O(3). Two of the vertices of the sulfate tetrahedra, O(1) and O(2), serve to link the Sn–O clusters into highly corrugated chains that extend along [010]. These chains are connected solely by hydrogen bonds that extend from two vertices of the clusters to the two remaining vertices of the sulfate tetrahedra: O(3) and O(4) (Fig. 3b).

Twinning of the Sn^{2+} sulfate

The Sn^{2+} sulfate crystal studied is interpreted to be a non-merohedral twin. Indeed, Ramik *et al.* (2003) noted on the basis of morphology that this compound generally seems to be twinned, although the thin plates examined in this study show sharp extinction. During data collection, we noted that some of the reflections on the CCD area detector are noticeably streaky (non-circular), although not clearly split, and some reflections seem to be consistent with a large cell with the b dimension double that presented in Table 1 (*i.e.,* ~25 Å). Solution and refinement in this large cell are not supported by the majority of the data, and resulted in systematically erroneous interatomic distances. Instead, the data were indexed and integrated using the cell presented in Table 1; use of the GEMINI twin-determination software (Bruker 1998b) did not resolve separate orientation-matrices for the twin components.

Solution and initial refinement of the structure resulted in six large peaks remaining in the difference-Fourier map. Inspection of the preliminary model, including the positions of the six large difference-Fourier peaks, in the structure-viewing program ATOMS (Dowty 2000) revealed that the six difference-peaks are offset from the six symmetrically independent Sn positions by approximately 1.75 Å (range 1.69–1.77 Å) along [$\bar{1}$03]. The six difference-peaks are related to the six positions of tin atoms by a rotation of 180° about [$\bar{1}$20] (Fig. 4). This twin relationship is supported by the results of analysis with the ROTAX program in the WINGX software suite (Cooper *et al.* 2001, Farrugia 1999).

In order to account for the effects of the non-merohedral twinning (in the absence of separate orientation-matrices for the twin components), the six difference-peaks were included in the refinement as Sn atoms, and their occupancy was refined with a single scale-factor. Although this procedure does not take into account the sulfur and oxygen atoms of the minor twin-domain, we consider it a reasonable approach, as more than three-quarters of the electron density in the compound is due to Sn atoms, and we thus account for the majority of the electron density present. The scale factor for these six "Sn atoms" refined to 9.0(1)% of a tin atom, 4.50(5) *epfu*, and the crystal was therefore interpreted to have a highly asymmetrical distribution of the two twin domains, with the major domain accounting for more than 90% of the scattering. The inclusion in the structure model of the difference peaks,

listed in Table 3 as positions A(1) – A(6), does not significantly affect the interatomic distances of the Sn, O and S positions.

DISCUSSION

Dodecahedral [$M_6\phi_8$] clusters

One of the most notable features of these structures is the presence of the [$Sn_6\phi_8$] deltoid dodecahedron, in which ϕ represents O^{2-} or (OH)$^-$. This cluster has been found in several stannous compounds (formulas are expressed to emphasize the presence of the [$Sn_6\phi_8$] cluster in each structure), including: ruthenium Sn^{2+} oxide, $Ru_3Sn_9[Sn_6O_8]O_6$ (Reichelt *et al.* 1995), osmium Sn^{2+} oxide, $Os_3Sn_9[Sn_6O_8]O_6$ (Söhnel & Reichelt 1997), Sn^{2+} methoxide, [$Sn_6O_4(OCH_3)_4$] (Harrison *et al.* 1978), and hydroromarchite, [$Sn_6O_4(OH)_4$] (Abrahams *et al.* 1996).

In aqueous solution, at relatively high concentrations of tin (0.001–0.02 mol/L Sn), the principal product of the hydrolysis of Sn^{2+} is the so-called trinuclear complex, [$Sn_3(OH)_4$]$^{2+}$ (*cf.* Sèby *et al.* 2001, Donaldson 1967). In crystal structures, this complex takes the form of a pseudotrigonal open cluster (*e.g.,* Donaldson *et al.* 1995). The [$Sn_6\phi_8$] dodecahedral cluster can be derived from two trinuclear complexes with facing bases (Fig. 5). As suggested by Sèby *et al.* (2001) for the trinuclear complex, it is possible that the dodecahedral cluster corresponds to a reaction intermediate that appears just prior to precipitation. Similar dodecahedral [$M_6\phi_8$] clusters (M = cation) occur in the structures of other heavy main-group elements with lone pairs of valence-shell electrons (*e.g.*, Pb^{2+} and Bi^{3+}). Selected examples include: lead oxyhydroxide, [$Pb_6O_4(OH)_4$] isostructural with hydroromarchite (Hill 1985), tetra-oxotetrahydroxohexabismuth perchlorate heptahydrate [$Bi_6O_4(OH)_4$](ClO_4)$_6$(H_2O)$_7$ (Sundvall 1982), and bismuth basic nitrate [$Bi_6O_{4.5}(OH)_{3.5}$]$_2$(NO_3)$_{11}$ (Henry *et al.* 2003). In the case of aqueous Bi^{3+}, the "hexanuclear" complex, [$Bi_6\phi_8$], is a major species

TABLE 7. BOND-VALENCE ANALYSIS FOR Sn^{2+} SULFATE (*vu*)

	S(1)	Sn(1)	Sn(2)	Sn(3)	Sn(4)	Sn(5)	Sn(6)	Total
O(1)	1.41	0.13			0.27	0.13		1.94
O(2)	1.30			0.15	0.26		0.15	1.86
O(3)	1.68							1.68
O(4)	1.48							1.48
O(5)		0.64			0.68		0.69	2.01
O(6)H		0.45	0.35				0.42	1.22
O(7)H			0.33	0.50		0.51		1.34
O(8)		0.79	0.75			0.75		2.29
O(9)			0.70	0.78			0.74	2.22
O(10)				0.75	0.78	0.67		2.20
Total	5.87	2.01	2.13	2.18	1.99	2.06	2.00	
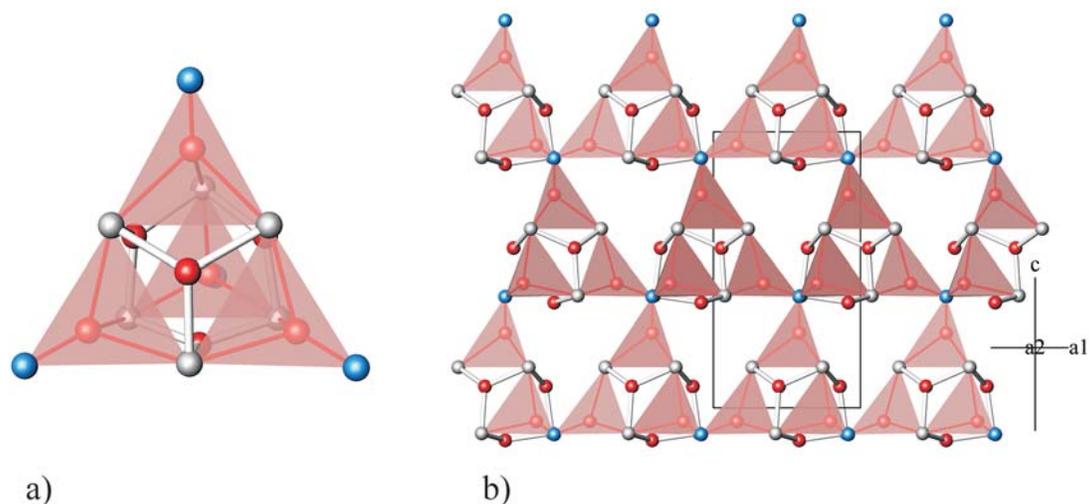
FIG. 2. a) A translucent "supertetrahedron" of four vertex-shared OSn_3Si tetrahedra. Four of the faces of the central octahedral cavity are decorated by oxygen in threefold coordination by tin atoms. b) Anion-centered representation of the structure, projected along [010]. The structure is a framework of decorated supertetrahedra, connected by silicon vertices. Atoms are displayed as in Figure 1, but the anion-centered tetrahedra are translucent pink, and bonds within the tetrahedra are red.
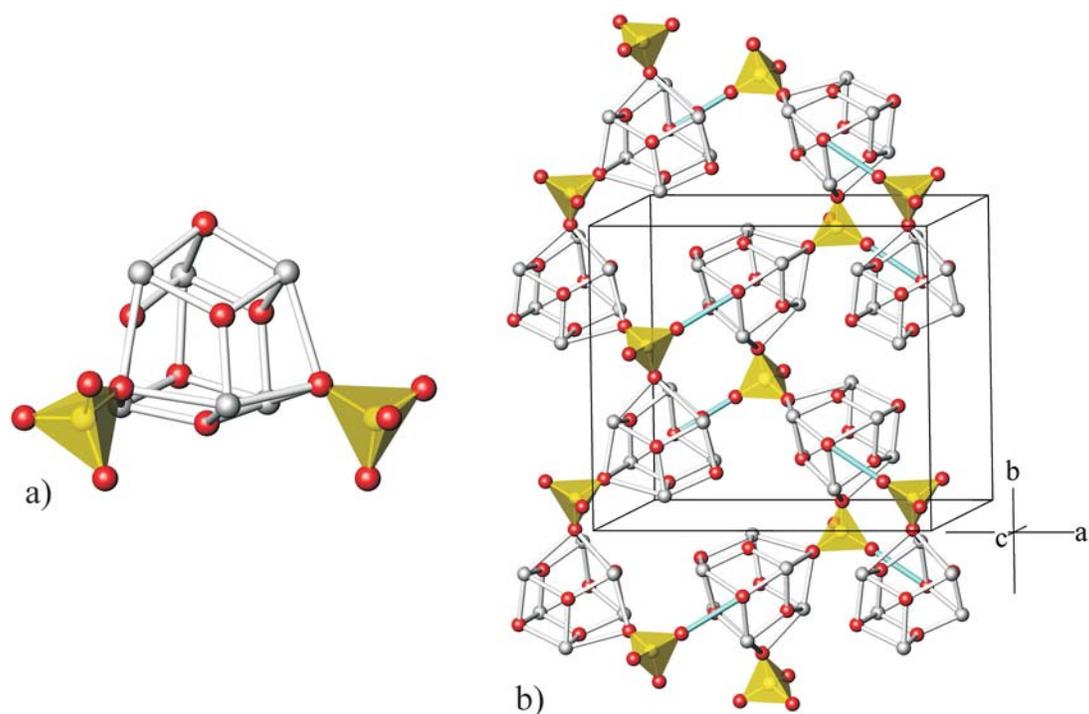
FIG. 3. a) A portion of the Sn^{2+} sulfate structure: the $[Sn_6O_6(OH)_2]$ cluster shown with two yellow sulfate tetrahedra. Sulfur is shown as yellow atoms. b) Clinographic projection of the structure along [001]. Highly corrugated chains of $[Sn_6O_6(OH)_2)]SO_2$ extend along [010]. Hydrogen bonding (shown as pale blue rods) connects the chains together.

in moderately acidic solutions over a wide range in concentration (Sundvall 1982), and thus by analogy it is conceivable that the $[Sn_6\phi_8]$ cluster might also occur as a species in solution.

There are several ways to view the structure of the $[Sn_6\phi_8]$ cluster. It may be derived by the amalgamation of two trinuclear complexes (Fig. 5). Alternatively, it has been considered to be similar to the structure of adamantane, $C_{10}H_{16}$. In this comparison, the cluster is formed by the addition of four bridging groups to a Sn_6O_4 adamantane-type skeleton (Harrison *et al.* 1978). The adamantane-type skeleton is geometrically identical to the As_4O_6 molecule found in arsenolite (Pertlik 1978) and the Sb_4O_6 molecule found in senarmontite (Svensson 1975); however, in the core of the $[Sn_6\phi_8]$ cluster, *i.e.,* Sn_6O_4, the roles of the cation and O atoms are reversed relative to those in arsenolite and senarmontite. In both heavy-metal compounds with the $[M_6\phi_8]$ cluster (M corresponds to Pb^{2+}, Bi^{3+}) and in the related molecular structures of arsenolite and senarmontite, the lone pairs of valence-shell electrons (LEP) are oriented into the voids or intermolecular spaces of the structures (pers. commun., E. Makovicky 2006). The compounds with the $[Sn_6\phi_8]$ cluster exhibit similar behavior, with the exception of the Os- and Ru-bearing compounds $Ru_3Sn_9[Sn_6O_8]O_6$ (Reichelt *et al.* 1995) and $Os_3Sn_9[Sn_6O_8]O_6$ (Söhnel & Reichelt 1997), in which the LEP serve to coordinate the platinum-group elements. We can thus consider a continuum of structures that have the $[M_6\phi_8]$ cluster, ranging from compounds held together by relatively weak forces (*e.g.*, hydrogen bonding in the case of hydroromarchite),

through structures containing LEP interactions (*e.g.*, $Ru_3Sn_9[Sn_6O_8]O_6$), to structures polymerized by strongly bonded polyhedra (*e.g.*, $[Sn_6O_8]Si$).

In a broader context, and perhaps of wider utility, is a comparison of the $[Sn_6\phi_8]$ cluster with portions of the structure of fluorite, CaF_2. In a representation of a single unit-cell of fluorite using anion-centered polyhedra (Fig. 6a), the structure consists of a *stella octangula* of eight edge-shared FCa_4 tetrahedra (Krivovichev 1999a, O'Keeffe & Hyde 1996), with apparent stoichiometry $Ca_{14}F_8$. By removing the eight Ca atoms at the vertices of the cubic unit-cell, we can emphasize the presence of the nominal Ca_6F_8 rhombic dodecahedron, {110} in point group *m3m*, at the core of the structure (Fig. 6b), and compare it to the $[Sn_6\phi_8]$ cluster that approximates a deltoid dodecahedron (Fig. 6c). The compounds with dodecahedral $[M_6\phi_8]$ clusters can thus be viewed as derivatives of fluorite, and can be compared to a wide range of fluorite-related structures (*cf.* Krivovichev 1999b, Krivovichev 2004).
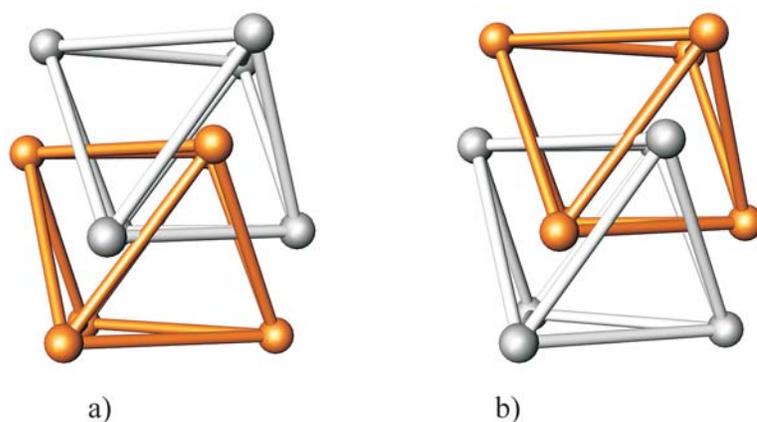
FIG. 4.   a) Perspective view of a portion of the Sn^{2+} sulfate structure, projected along [$\bar{1}20$]. The six tin positions are shown in gray, and approximate the vertices of an octahedron. The six large difference-Fourier peaks are shown in orange and form a similar octahedron. b) The tin positions and difference-Fourier peaks after a rotation of 180° about [$\bar{1}20$].

FIG. 5.   a) Two trinuclear complexes, $[Sn_3(OH)_4]^{2+}$, with facing bases. b) The $[Sn_6\phi_8]$ cluster (ϕ: O^{2-} or OH^-). Legend is the same as in Figure 1.
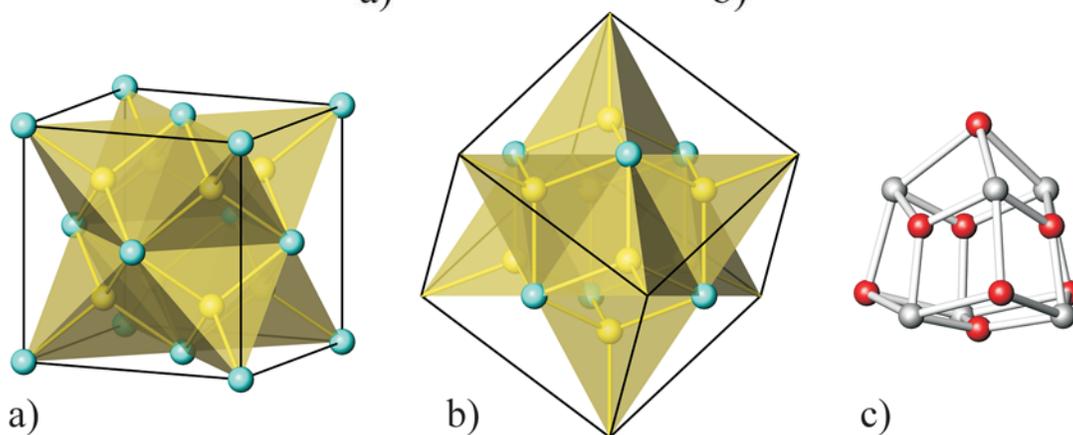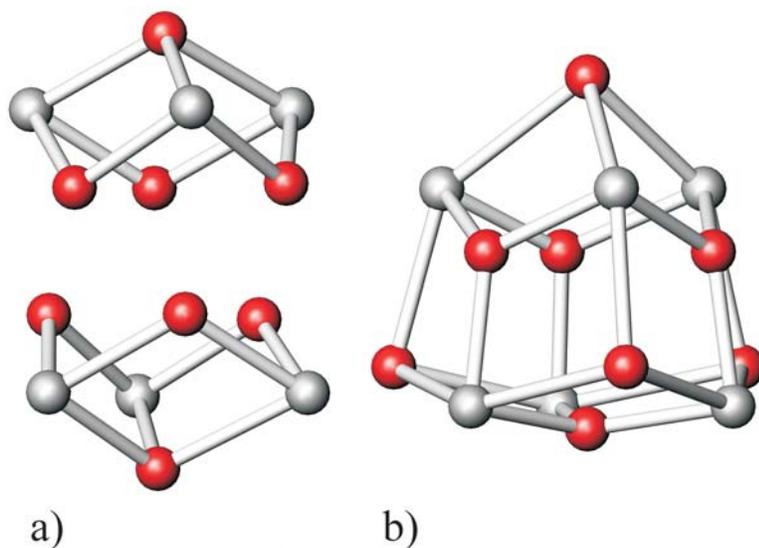
FIG. 6.   a) The structure of fluorite, CaF_2, displayed as a *stella octangula* of eight translucent edge-sharing FCa_4 tetrahedra. Fluorine atoms are shown in yellow, calcium atoms in blue-green. b) A portion of the structure of fluorite, projected along [213]. The eight calcium atoms at the corners of the stella octangula have been removed, and the projection changed, to emphasize the presence of the Ca_6F_8 rhombic dodecahedron at the core of the structure. c) The $[Sn_6\phi_8]$ cluster (ϕ: O^{2-} or OH^-), which approximates a deltoid dodecahedron, shown in a similar orientation.

REFERENCES

ABRAHAMS, I., GRIMES, S.M., JOHNSTON, S.R. & KNOWLES, J.C. (1996): Tin(II) oxyhydroxide by X-ray powder diffraction. *Acta Crystallogr.* **C52**, 286-288.

BINDI, L., EVAIN, M. & MENCHETTI, S. (2006): Temperature dependence of the silver distribution in the crystal structure of natural pearceite, $(Ag,Cu)_{16}(As, Sb)_2S_{11}$. *Acta Crystallogr.* **B62**, 212-219.

BRESE, N.E. & O'KEEFFE, M. (1991): Bond-valence parameters for solids. *Acta Crystallogr.* **B47**, 192-197.

BRUKER (1998a): SAINT, V 5.01 program for reduction of data collected on Bruker AXS CCD area detector systems. Bruker Analytical X-Ray Systems, Madison, Wisconsin.

BRUKER (1998b): GEMINI, twinning solution program suite. Bruker Analytical X-Ray Systems, Madison, Wisconsin.

ČERNÝ, P., FRANSOLET, A.-M., ERCIT, T.S. & CHAPMAN, R. (1988): Foordite $SnNb_2O_6$, a new mineral species, and the foordite–thoreaulite series. *Can. Mineral.* **26**, 889-898.

COOPER, R.I., GOULD, R.O., PARSONS, S. & WATKIN, D.J. (2001): The derivation of non-merohedral twin laws during refinement by analysis of poorly fitting intensity data and the refinement of non-merohedrally twinned crystals structures in the program CRYSTALS. *J. Appl. Crystallogr.* **35**, 168-174.

DAVIES, C.G. & DONALDSON, J.D. (1967): Basic tin(II) sulphates. *J. Chem. Soc.* **A11**, 1790-1793.

DONALDSON, J.D. (1964): *A Review of the Chemistry of Tin(II) Compounds.* Tin Research Institute, Perivale, Greenford, Middlesex, U.K.

DONALDSON, J.D. (1967): The chemistry of bivalent tin. *Prog. Inorg. Chem.* **8**, 287-356.

DONALDSON, J.D., GRIMES, S.M., JOHNSTON, S.R. & ABRAHAMS, I. (1995): Characterisation of the tin(II) hydroxide cation $[Sn_3(OH)_4]^{2+}$, and the crystal structure of tritin(II) tetrahydroxide dinitrate. *J. Chem. Soc., Dalton Trans.* **13**, 2273-2276.

DONALDSON, J.D., MOSER, W. & SIMPSON, W.B. (1961): Red tin(II) oxide. *J. Chem. Soc.*, 839-841.

DONALDSON, J.D., MOSER, W. & SIMPSON, W.B. (1963): The structure of the red modification of tin(II) oxide. *Acta Crystallogr.* **16**, suppl., A22.

DOWTY, E. (2000): *ATOMS for Windows and Macintosh, version 5.1,* Shape Software, Kingsport, Tennessee.

DUNKLE, S.E., CRAIG, J.R. & LUSARDI, W.R. (2004): Romarchite and associated phases as common corrosion products on pewter artifacts from marine archaeological sites. *Geoarchaeology* **19**, 531-552.

DUNKLE, S.E., CRAIG, J.R., RIMSTIDT, J.D. & LUSARDI, W.R. (2003): Romarchite, hydroromarchite and abhurite formed during the corrosion of pewter artifacts from the *Queen Anne's Revenge* (1718). *Can. Mineral.* **41**, 659-669.

EDWARDS, R., GILLARD, R.D. & WILLIAMS, P.A. (1996): The stabilities of secondary tin minerals. 2. The hydrolysis of tin(II) sulphate and the stability of $Sn_3O(OH)_2SO_4$. *Mineral. Mag.* **60**, 427-432.

FARRUGIA, L.J. (1999): WINGX suite for small-molecule single-crystal crystallography. *J. Appl. Crystallogr.* **32**, 837-838.

GARRELS, R.M. & CHRIST, C.L. (1965): *Solutions, Minerals, and Equilibria.* Harper & Row, New York, N.Y.

GARUTI, G. & ZACCARINI, F. (2005): Minerals of Au, Ag and U in volcanic-rock-associated massive sulfide deposits of the Northern Appenine ophiolite, Italy. *Can. Mineral.* **43**, 935-950.

GRIMVALL, S. (1975): The crystal structure of $Sn_3O(OH)_2SO_4$. *Acta Chem. Scand.* **A29**, 590-598.

HARRISON, P.G. (1998): Compounds of tin: general trends. *In* Chemistry of Tin (2nd ed., P.J. Smith, editor). Blackie, New York, N.Y. (10-61).

HARRISON, P.G., HAYLETT, B.G. & KING, T.J. (1978): X-ray crystal structure of $Sn_6O_4(OMe)_4$: an intermediate in the hydrolysis of tin(II) dimethoxide. *J. Chem. Soc., Chem. Commun.*, 112-113.

HENRY, N., EVAIN, M., DENIARD, P., JOBIC, S., MENTRÉ, O. & ABRAHAM, F. (2003): $[Bi_6O_{4.5}(OH)_{3.5}]_2(NO_3)_{11}$: a new anhydrous bismuth basic nitrate. Synthesis and structure determination from twinned crystals. *J. Solid State Chem.* **176**, 127-136.

HILL, R.J. (1985): Structure of $Pb_3O_2(OH)_2$ by Rietveld analysis of neutron powder diffraction data. *Acta Crystallogr.* **C41**, 998-1003.

KRIVOVICHEV, S.V. (1999a): Systematics of fluorite-related structures. I. General principles. *Solid State Sci.* **1**, 211-219.

KRIVOVICHEV, S.V. (1999b): Systematics of fluorite-related structures. II. Structural diversity. *Solid State Sci.* **1**, 221-231.

KRIVOVICHEV, S.V. (2004): Crystal structures and cellular automata. *Acta Crystallogr.* **A60**, 257-262.

KRIVOVICHEV, S.V. & FILATOV, S.K. (1999a): Metal arrays in structural units based on anion-centered metal tetrahedra. *Acta Crystallogr.* **B55**, 664-676.

KRIVOVICHEV, S.V. & FILATOV, S.K. (1999b): Structural principles for minerals and inorganic compounds containing anion-centered tetrahedra. *Am. Mineral.* **84**, 1099-1106.

LE PAGE, Y. (1987): Computer derivation of the symmetry elements implied in a structure description. *J. Appl. Crystallogr.* **20**, 264-269.

LIVINGSTONE, D.A. (1963): Chemical composition of rivers and lakes. *U.S. Geol. Surv., Prof. Pap.* **440-G**.

MANDARINO, J.A. & BACK, M.E. (2004): *Fleischer's Glossary of Mineral Species 2004*. The Mineralogical Record Inc., Tucson, Arizona.

NICKEL, E.H. (1995): Definition of a mineral. *Can. Mineral.* **33**, 689-690.

NICKEL, E.H. & GRICE, J.D. (1998): The IMA Commission on New Minerals and Mineral Names: procedures and guidelines on mineral nomenclature, 1998. *Can. Mineral.* **36**, 913-926.

O'KEEFFE, M. & HYDE, B.G. (1996): Crystal Structures. I. Patterns and Symmetry. *Mineral. Soc. Am., Monogr.* **3**.

ORGAN, R.M. & MANDARINO, J.A. (1971): Romarchite and hydroromarchite, two new stannous minerals. *Can. Mineral.* **10**, 916 (abstr.).

PERTLIK, F. (1978): Structure refinement of cubic As_2O_3 (arsenolite) with single crystal data. *Czech. J. Phys.* **28**, 170-176.

RAMIK, R.A. (2004): Soak in water and refrigerate for 160 years: a recipe for corrosion. *Archaeological Newsletter* (*Royal Ontario Museum*), *Ser.* **III**, *No.* 16, 1-4.

RAMIK, R.A., ORGAN, R.M. & MANDARINO, J.A. (2003): On type romarchite and hydroromarchite from Boundary Falls, Ontario, and notes on other occurrences. *Can. Mineral.* **41**, 649-657.

REICHELT, W., SÖHNEL, T., RADEMACHER, O., OPPERMANN, H., SIMON, A., KÖHLER, J. & MATTAUSCH, H.-J. (1995): Condensed $RuSn_6$ octahedra in $Ru_3Sn_{15}O_{14}$. *Angew. Chem.* (*International Ed.*) **34**, 2113-2114.

RUDNICK, R.L. & GAO, S. (2003): The composition of the continental crust. *In* Treatise on Geochemistry **3** (H.D. Holland & K.K. Turekian, eds.). Elsevier-Pergamon, Oxford, U.K. (1-64).

SCHENK, H. (1984): *An Introduction to Direct Methods. The Most Important Phase Relationships and their Application in Solving the Phase Problem*. International Union of Crystallography, Commission on Crystallographic Teaching, Teaching Pamphlet 17. University College Cardiff Press, Cardiff, Wales, 27 p., www.iucr.org

SÈBY, F., POTIN-GAUTIER, M., GIFFAULT, E. & DONARD, O.F.X. (2001): A critical review of thermodynamic data for inorganic tin species. *Geochim. Cosmochim. Acta* **65**, 3041-3053.

SHELDRICK, G.M. (1998): *SHELXTL NT, V5.1, Program Suite for Solution and Refinement of Crystal Structures*. Bruker Analytical X-ray Systems, Madison, Wisconsin.

SÖHNEL, T. & REICHELT, W. (1997): $Os_3Sn_{15}O_{14}$, ein ternäres Oxid mit osmiumgefüllten Sn_6-Oktaedern. *Acta Crystallogr.* **C53**, 9-11.

SPEK, A.L. (2003): Single-crystal structure validation with the program PLATON. *J. Appl. Crystallogr.* **36**, 7-13.

SUNDVALL, B. (1982): Crystal structure of tetraoxotetra hydroxohexabismuth(III) perchlorate heptahydrate, $Bi_6O_4(HO)_4(ClO_4)_6 \cdot 7H_2O$: an X-ray and neutron diffraction study. *Inorg. Chem.* **22**, 1906-1912.

SVENSSON, C. (1975): Refinement of the crystal structure of cubic antimony trioxide, Sb_2O_3. *Acta Crystallogr.* **B31**, 2016-2018.

VON SCHNERING, H.G., NESPER, R. & PELSHENKE, H. (1981): $Sn_{21}Cl_{16}(OH)_{14}O_6$, das sogennante basischen Zinn(II)-chloride. *Z. Naturforsch. B. Anorg. Chem., Org. Chem.* **36**, 1551-1560.

WILSON, A.J.C., ed. (1992): *International Tables for X-ray Crystallography, Vol. C*. Kluwer Academic Press, Boston, Massachusetts.